

# Journal of Materials Chemistry C

Accepted Manuscript



This is an *Accepted Manuscript*, which has been through the Royal Society of Chemistry peer review process and has been accepted for publication.

*Accepted Manuscripts* are published online shortly after acceptance, before technical editing, formatting and proof reading. Using this free service, authors can make their results available to the community, in citable form, before we publish the edited article. We will replace this *Accepted Manuscript* with the edited and formatted *Advance Article* as soon as it is available.

You can find more information about *Accepted Manuscripts* in the [Information for Authors](#).

Please note that technical editing may introduce minor changes to the text and/or graphics, which may alter content. The journal's standard [Terms & Conditions](#) and the [Ethical guidelines](#) still apply. In no event shall the Royal Society of Chemistry be held responsible for any errors or omissions in this *Accepted Manuscript* or any consequences arising from the use of any information it contains.

(manuscript submitted to Journal of Materials Chemistry C, May 2015)

## Thermodynamic stability of lead-free alkali niobate and tantalate perovskites

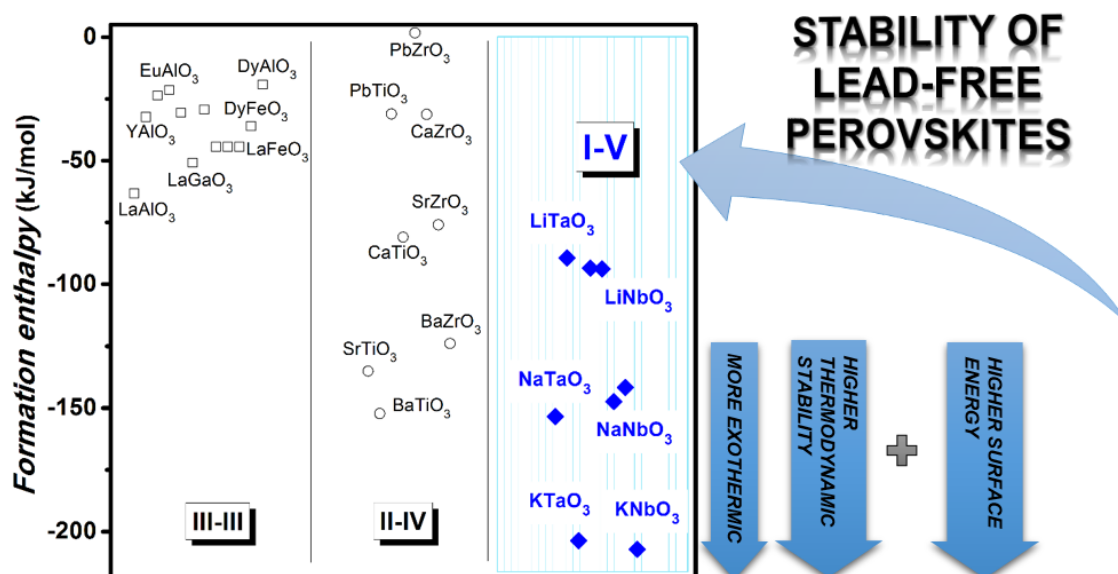
Sulata K. Sahu<sup>1</sup>, Sebastian Zlotnik<sup>2</sup>, Alexandra Navrotsky<sup>1</sup> and Paula M. Vilarinho<sup>2\*</sup>

<sup>1</sup> Peter A. Rock Thermochemistry Laboratory and NEAT ORU, University of California Davis, Davis, CA 95616, USA

<sup>2</sup> Department of Materials and Ceramic Engineering, CICECO – Aveiro Materials Institute, University of Aveiro, 3810-193 Aveiro, Portugal

\* corresponding author: [paula.vilarinho@ua.pt](mailto:paula.vilarinho@ua.pt)

TOC



## Abstract

Lead free niobates and tantalates currently form one of the most promising groups of ferroelectrics, piezoelectrics and related materials, with important applications for the next generation of lead free sensors, actuators and microelectromechanical systems (MEMs). In view of their importance, the enthalpies of formation from binary oxide components at 25 °C, measured by high temperature oxide melt solution calorimetry of a set of alkali tantalates and niobates with perovskite-like structures, LiTaO<sub>3</sub>, LiNbO<sub>3</sub>, NaTaO<sub>3</sub>, NaNbO<sub>3</sub> and KNbO<sub>3</sub> are reported to be  $-93.74 \pm 1.77$ ,  $-93.44 \pm 1.48$ ,  $-147.35 \pm 2.46$ ,  $-141.63 \pm 2.27$  and  $-207.12 \pm 1.74$  kJ/mol for LiTaO<sub>3</sub>, LiNbO<sub>3</sub>, NaTaO<sub>3</sub>, NaNbO<sub>3</sub> and KNbO<sub>3</sub>, respectively. The surface energies of nanocrystalline perovskites of these alkali tantalates and niobates were experimentally determined for the first time by calorimetry. The energies of the hydrated surface are  $1.04 \pm 0.34$ ,  $1.21 \pm 0.78$ ,  $1.58 \pm 0.29$ ,  $2.16 \pm 0.57$  and  $2.95 \pm 0.59$  J/m<sup>2</sup> for LiTaO<sub>3</sub>, LiNbO<sub>3</sub>, NaTaO<sub>3</sub>, NaNbO<sub>3</sub> and KNbO<sub>3</sub>, respectively. The stability of the lead-free perovskites of I-V type is discussed based on their tolerance factor and acid-base chemistry. The formation enthalpy becomes more exothermic (higher thermodynamic stability) and surface energy increases (greater destabilization for a given particle size) with increase in ionic radius of the A-site cation (Li, Na and K) and with increasing tolerance factor. These correlations provide key insights into how lead free niobates and tantalates behave during synthesis and processing; i.e they explain, for example, why KNbO<sub>3</sub> and KTaO<sub>3</sub> nanoparticles will be thermodynamically more reactive than their Li and Na counterparts. This understanding will facilitate the development of optimized processing techniques and applications.

**Keywords:** perovskite, alkali niobates, tantalates, KNbO<sub>3</sub>, NaTaO<sub>3</sub>, NaNbO<sub>3</sub>, LiTaO<sub>3</sub>, LiNbO<sub>3</sub>, KTaO<sub>3</sub>, calorimetry, formation enthalpy, phase stability, surface energy

## 1. Introduction

Due to recent demands for environmental friendly components and continuous developments of functional materials for current and future technologies, perovskite oxides are highly attractive compounds because of their remarkable properties important for various technological applications. Ecologically driven needs for less toxic materials leads to the search

for alternatives to lead-based systems, the family of alkali based perovskite tantalates and niobates being potentially strategic candidates.

Among this group of materials with general formula  $A(\text{Ta or Nb})\text{O}_3$  (where  $A$  stands for alkali metal), perovskite tantalates,  $\text{NaTaO}_3$ ,  $\text{LiTaO}_3$  and  $\text{KTaO}_3$ , and niobates,  $\text{NaNbO}_3$ ,  $\text{LiNbO}_3$  and  $\text{KNbO}_3$ , possess unique features for a number of applications.  $\text{NaTaO}_3$  and  $\text{NaNbO}_3$  exhibit a rich polymorphism over a wide range of temperatures, and possess attractive physical properties to be used as components in ferroelectric and piezoelectric applications, photocatalysts in water splitting, pollutant degradation, and thermoelectric materials<sup>1-5</sup>. Both  $\text{LiTaO}_3$  and  $\text{LiNbO}_3$  are  $\text{ABO}_3$ -type ferroelectrics (with high Curie points,  $T_C$ ;  $>600$  °C for  $\text{LiTaO}_3$  and  $>1100$  °C for  $\text{LiNbO}_3$ ) and are relevant materials in electro-optic applications due to high electro-optic coefficient, optical damage resistance and low loss<sup>6-8</sup>.  $\text{KNbO}_3$  is a widely studied ferroelectric (analogous to  $\text{BaTiO}_3$  in terms of structural transitions) due to its large piezoelectric constant, electromechanical coupling coefficient, electro-optic coefficient and nonlinear optical coefficient<sup>9-11</sup>; and  $\text{KTaO}_3$  is an attractive dielectric material (also an incipient ferroelectric and a quantum paraelectric)<sup>12</sup> with very low microwave losses<sup>13</sup>. Moreover, solid solutions of  $\text{KNbO}_3$  and  $\text{NaNbO}_3$ ,  $(\text{K}_{1-x}\text{Na}_x)\text{NbO}_3$  (KNN) are currently being considered as a potential substitute for the present piezoelectric market leader,  $\text{Pb}(\text{Zr}_{1-x}\text{Ti}_x)\text{O}_3$  (PZT)<sup>14</sup>. KNN has a relatively high  $T_C \approx 420$  °C, which is a considerable advantage over PZT<sup>15</sup>, and good piezoelectric properties<sup>16, 17</sup>. Other type of solid solutions composed of  $\text{KNbO}_3$  and  $\text{KTaO}_3$ ,  $\text{K}(\text{Ta}_{1-y}\text{Nb}_y)\text{O}_3$  (KTN) are also recognized as a system with high potential for nonlinear electro-optical devices, e.g. a light beam modulator and deflector, due to relatively large electro-optic coefficients measured in single crystals:  $\gamma_{33} = 216.7$  pm/V,  $\gamma_{13} = -21.2$  pm/V, and  $\gamma_c = 242.9$  pm/V (1 kHz)<sup>18</sup>.

It is well known that processing single crystal and polycrystalline alkali tantalates and niobates is not trivial and some difficulties accompany the syntheses. The two most relevant problems are the moisture sensitivity of alkali precursors<sup>16, 17, 19</sup> and the considerable losses in alkali element content during synthesis at high temperature (due to their high vapour pressures)<sup>16, 20, 21</sup> which lead to compositional fluctuations. In addition, material stability (mechanical, thermal or chemical) is always a key aspect to ensure the durability of the device in which it is used<sup>22</sup>. Considering that the chemical and thermal stabilities of materials are strongly related to the formation energy of the compound<sup>23-26</sup>, it is then crucial to know their thermodynamic properties to better control the processing parameters and, ultimately, the functional properties. However, there are only few data on enthalpy of formation and transitions

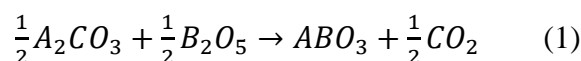
on selected compounds ( $\text{LiNbO}_3$  and  $\text{NaNbO}_3$ ) within the group of alkali tantalates and niobates<sup>27, 28 29, 30</sup>. Moreover, there is recent scientific interest in nanoparticles with perovskite-type structure due to the appearance of novel phenomena at the nanoscale. An example is absence of ferroelectricity in nanocrystalline  $\text{BaTiO}_3$ <sup>31</sup>. Surfaces and interfaces play a crucial role in many processes in solids, i.e. chemical reactivity, catalysis, coarsening, sintering, polymorphic stability, and their energies are directly related to the driving forces for these phenomena<sup>32, 33</sup>. Many theoretical calculations of the energies of variously oriented surfaces, interfaces, and grain boundaries have been reported<sup>34-36</sup>, but there are only few experimental determinations due to the difficulties in such measurements. However, surface energies of nanomaterials have been successfully determined by using a calorimetric approach<sup>37-41</sup>. Progress in calorimetry technique and developments in metrology over the past two decades have provided opportunity to collect extensive thermodynamic data on various systems<sup>42-44</sup>. High-temperature oxide melt solution calorimetry has been successfully demonstrated to measure the surface energies of an array of binary and ternary oxides directly<sup>41, 45, 46</sup> but not yet for alkali tantalate and niobate perovskites.

In this paper a systematic study of the formation and surface enthalpies of  $\text{LiNbO}_3$ ,  $\text{LiTaO}_3$ ,  $\text{NaNbO}_3$ ,  $\text{NaTaO}_3$  and  $\text{KNbO}_3$ , is presented. The results are discussed in terms of the effect of different alkali metals on the A-site of the perovskites. The samples were synthesized by the mixed oxide method, and calcined at relatively low temperature to ensure the synthesis of nanocrystalline powders. Enthalpies of the hydrated surfaces were determined using calorimetric measurements. These experimentally obtained data support discussion of surface processing phenomena, giving insights on nucleation, phase stability, sintering behaviour and mass transport.

## 2. Experimental

### (1) Synthesis

Perovskites were prepared via conventional solid state reaction, according to the reaction:



where *A* stands for alkali metal: Li, Na or K, and *B* for: Ta or Nb. The sources of alkali metals were metal carbonates: K<sub>2</sub>CO<sub>3</sub> (Merck, 99 %), Li<sub>2</sub>CO<sub>3</sub> (Merck, 99 %), Na<sub>2</sub>CO<sub>3</sub> (Chempur, ≥ 99.5 %), and transition metal oxides: Ta<sub>2</sub>O<sub>5</sub> (Aldrich, 99 %) and Nb<sub>2</sub>O<sub>5</sub> (Chempur, 99.9 %). Planetary ball milling at 200 rpm for 8 h was used to homogenize the reagents prior to calcination at 800 – 850 °C for 5 h with heating and cooling rates of 5 °C/min.

## (2) Characterization

XRD patterns of the synthesized powders were recorded using a Bruker-AXS D8 Advance diffractometer (Bruker-AXS Inc.) operated at an accelerating voltage of 40 kV and an emission current of 40 mA with CuK $\alpha$  radiation ( $\lambda = 0.15406$  nm). Data were acquired from 20 to 70° 2 $\theta$  with a step size of 0.03° and a collection time of 0.5 s/step. Crystalline phases were identified using Jade 6.1 software (Materials Data Inc.). The crystallite size of the samples was calculated from the diffraction peak broadening using a whole profile fitting procedure (Pawley method)<sup>47</sup> as implemented in Jade 6.1.

The compositions of the synthesized samples were measured (in bulk ceramics) using wavelength dispersive electron probe microanalysis with a Cameca SX100 instrument operated at an accelerating voltage of 15 kV, a beam current of 20 nA, and a beam size of 1  $\mu$ m; the sintered pellets were polished and carbon coated, and the compositions were estimated from an average of 10 data points per sample. The elemental composition of the Li-containing powders was analysed by inductively coupled plasma mass spectrometry. 1.5 to 2.0 mg of each sample was dissolved in 40 mL of a mixture of 3 % HNO<sub>3</sub> (prepared from concentrated nitric acid, 70 %, EMD Chemicals by dilution using 18.2 mohm water) + 10 ml of 2 % HF (prepared from concentrated hydrofluoric acid, EM Science 48 % by dilution using 18.2 mohm water). The analyses were performed using an Agilent 7500CE ICP-MS.

The specific surface area,  $S_{\text{BET}}$ , of the prepared powders was evaluated by the Brunauer-Emmett-Teller (BET) method, using N<sub>2</sub> as the adsorbate gas at -197 °C. Ten-point nitrogen adsorption isotherms were collected in a relative pressure range of  $p/p^0 = 0.05 - 0.3$  (where,  $p^0$  is the saturation pressure) using a Micromeritics ASAP 2020 surface area and porosity analyzer. Prior to the analysis, the samples were degassed under vacuum at 300 °C for 2 h. The uncertainties in the BET surface area measurements were propagated from fitting a straight line to  $1/[Q(p^0/p_1)]$  ( $Q$  is the adsorbed quantity, mmol/g) vs  $p/p^0$  using the Micromeritics software. The total amount of water on the nanocrystalline samples was determined on a set of five samples, each 10 – 15 mg, by thermogravimetric analysis using a Netzsch STA 449 system.

The sample was heated at 10 °C/min in a platinum crucible from 30 to 900 °C in an oxygen atmosphere. A buoyancy correction was made by subtracting the baseline, collected by running an identical scan with an empty platinum crucible. The water content was determined from the weight loss curve.

### (3) High-Temperature Oxide Melt Solution Calorimetry

The drop solution enthalpies of the samples were measured in a custom-made isoperibol Tian-Calvet twin microcalorimeter described previously<sup>48</sup>. The calorimeter assembly was flushed with oxygen at 43 mL/min, and oxygen was bubbled through the solvent at 4.5 mL/min to aid dissolution and maintain oxidizing conditions. Pellets of approximately 5 mg were loosely pressed, weighed, and dropped from room temperature into 3Na<sub>2</sub>O · 4MoO<sub>3</sub> molten solvent at 702 °C. Measurements were repeated eight times for each sample to achieve statistically reliable data. The calorimeter was calibrated against the heat content of 5 mg pellets of high purity  $\alpha$ -Al<sub>2</sub>O<sub>3</sub> (Alfa Aesar, 99.997 %) dropped into an empty crucible. Surface energy calculations from high-temperature drop solution calorimetry data were completed according to methods of earlier studies<sup>49-51</sup>.

## 3. Results and discussion

### (1) Phase composition, structural and microstructural characterization

The as-synthesized set of alkali tantalate and niobate samples were analysed by XRD in the 2 $\theta$  range of 20 – 70 ° (Figure 1), and in all cases monophasic patterns were detected within a detection limit of about 2 % of a second phase. XRD patterns match the following JCPDS-PDF files: rhombohedral LiTaO<sub>3</sub> to 01-087-2461 (SG (space group): *R3c*), rhombohedral LiNbO<sub>3</sub> to 04-009-3436 (SG: *R3c*), orthorhombic NaTaO<sub>3</sub> to 04-010-2738 (SG: *Pnma*), orthorhombic NaNbO<sub>3</sub> to 04-014-2322 (SG: *Pbcm*) and orthorhombic KNbO<sub>3</sub> to 04-007-9572 (SG: *Bmm2*). The refined average crystallite size (diameter),  $\langle D \rangle$ , for LiTaO<sub>3</sub>, LiNbO<sub>3</sub>, NaTaO<sub>3</sub>, NaNbO<sub>3</sub> and KNbO<sub>3</sub> is given in Table 1.

According to ICP-MS LiTaO<sub>3</sub> and LiNbO<sub>3</sub> have compositions Li<sub>1.002±0.004</sub>Ta<sub>0.998±0.004</sub>O<sub>3</sub> and Li<sub>1.003±0.006</sub>Nb<sub>0.997±0.004</sub>O<sub>3</sub>, whereas NaTaO<sub>3</sub>, NaNbO<sub>3</sub> and KNbO<sub>3</sub> as determined by microprobe (EPMA), are Na<sub>0.999±0.006</sub>Ta<sub>1.001±0.007</sub>O<sub>3±0.002</sub>, Na<sub>0.998±0.009</sub>Nb<sub>1.002±0.009</sub>O<sub>3±0.008</sub> and

$\text{K}_{0.998\pm 0.003}\text{Nb}_{1.002\pm 0.003}\text{O}_{3\pm 0.009}$ , respectively. Within the experimental errors the prepared compounds are stoichiometric and the nominal compositions are used in the thermodynamic calculations.

BET surface areas,  $S_{BET}$ , of the nanocrystalline alkali tantalates and niobates are shown in Table 1. The  $S_{BET}$  ranges from 4.17 to 8.97 m<sup>2</sup>/g. Additionally the crystallite size from BET surface area was calculated, assuming spherical crystallites (which is reasonable because of the relatively isotropic nanoparticles). The  $\langle D \rangle$  from BET surface ranges from 31.5 to 106.2 nm. The crystallite diameters calculated from BET surface area are similar to those from XRD, indicating that there is no significant agglomeration in the nanocrystalline samples.

## (2) Calculation of surface and formation enthalpies

The measured average drop solution enthalpies ( $\Delta H_{ds}$ ) of bulk and nano LiTaO<sub>3</sub>, LiNbO<sub>3</sub>, NaTaO<sub>3</sub>, NaNbO<sub>3</sub> and KNbO<sub>3</sub> are given in Table 1. The difference between the enthalpy of drop solutions,  $\Delta H_{ds}$ , of the bulk and nano samples, corrected for water content, arises from the surface enthalpy term ( $\gamma_{hyd} SA$ , where SA is the surface area and  $\gamma_{hyd}$  is the surface enthalpy of the hydrated surface), essentially equivalent to the surface energy and as argued previously, very similar to the surface free energy<sup>46</sup>. The  $\gamma_{hyd}$  is calculated as the difference between the drop solution enthalpies of macroscopic (bulk) and nanosized (nano) materials, divided by the difference in surface area:

$$\gamma_{hyd} = \frac{\Delta H_{ds} (bulk) - \Delta H_{ds} (nano)}{S_{BET}} \quad (2)$$

where  $\gamma_{hyd}$  represents the surface enthalpy of the hydrated surface,  $\Delta H_{ds}$  stands for the drop solution enthalpy and  $S_{BET}$  is the surface area. Since all nanocrystalline samples contain adsorbed water on their surfaces, the  $\Delta H_{ds}$  values were corrected for water content following procedures described previously<sup>41, 50</sup>. The thermochemical cycle used for water correction for nanosized samples is given in Table 2. The energy of the hydrated surface is  $1.04 \pm 0.34$ ,  $1.21 \pm 0.78$ ,  $1.58 \pm 0.29$ ,  $2.16 \pm 0.57$  and  $2.95 \pm 0.59$  J/m<sup>2</sup> for LiTaO<sub>3</sub>, LiNbO<sub>3</sub>, NaTaO<sub>3</sub>, NaNbO<sub>3</sub> and KNbO<sub>3</sub>, respectively. The measured surface energies refer to the real samples having a range of surface planes and defect structures.

Table 3 presents the thermochemical cycles used to determine the formation enthalpies of LiTaO<sub>3</sub>, LiNbO<sub>3</sub>, NaTaO<sub>3</sub>, NaNbO<sub>3</sub> and KNbO<sub>3</sub> perovskites both from oxides and elements. The formation enthalpies of LiTaO<sub>3</sub>, LiNbO<sub>3</sub>, NaTaO<sub>3</sub>, NaNbO<sub>3</sub> and KNbO<sub>3</sub> from constituent

oxides  $\Delta H_f^{\text{ox}}$  at 25 °C are  $-93.74 \pm 1.82$ ,  $-93.44 \pm 1.55$ ,  $-147.35 \pm 2.50$ ,  $-141.63 \pm 2.40$  and  $-207.12 \pm 1.85$  kJ/mol, respectively. The formation enthalpies of alkali tantalate and niobate perovskites become more exothermic with increase in the size of the alkali cations, however for a given alkali cation, the niobate and tantalate perovskite have comparable energetics. LiNbO<sub>3</sub> has a reported enthalpy of formation from constituent oxides of  $-98.33 \pm 1.70$  kJ/mol<sup>27</sup> and NaNbO<sub>3</sub> has reported enthalpy of formation of  $-153.46 \pm 2.33$  kJ/mol<sup>27</sup> and  $-157.40 \pm 2.2$  kJ/mol<sup>30</sup>, in good agreement with our present values. Formation enthalpy of NaNbO<sub>3</sub>,  $\Delta H_f^{\circ}$  (NaNbO<sub>3</sub>) was determined by Popovič *et al.*<sup>28</sup> and Kobertz *et al.*<sup>29</sup> using Knudsen effusion mass spectrometry and are found to be  $-1220$  kJ/mol and  $-1250.8 \pm 7$  kJ/mol, respectively. These values of  $\Delta H_f^{\circ}$  matches well with our results. The  $\Delta H_f^{\circ}$  of LiNbO<sub>3</sub>, NaNbO<sub>3</sub> and KNbO<sub>3</sub> at 25 °C was calculated by Shigemi *et al.*<sup>34-36</sup> using a plane-wave pseudopotential method within a density functional formalism, and were found to be  $-1327.70$  (rhombohedral *R3c*),  $-1291.04$  (orthorhombic *Pbma*) and  $-1306.04$  kJ/mol (orthorhombic *Bmm2*), Körbel *et al.*<sup>52</sup> calculated the  $\Delta H_f^{\circ}$  to be  $-1336.51$  and  $-1378.97$  kJ/mol for NaNbO<sub>3</sub> and KNbO<sub>3</sub>, respectively. These values agree well with our formation enthalpies derived using calorimetric techniques. Reznitskii<sup>53</sup> calculated the heat of reaction using the enthalpies of changes,  $\Sigma\delta H$ , in the cation coordination number,  $\Delta H_f^{\text{ox}} = -31.3 + 0.84 \cdot \Sigma\delta H$  (kJ/mol), or from the function  $\Delta H_f^{\text{ox}} = 2[-60 + 500 \cdot (1 - t)]$  (kJ/mol); the calculated values were  $-150.00 \pm 60$ ,  $-150.00 \pm 60$ ,  $-206.00 \pm 26$  and  $-206.00 \pm 22$  kJ/mol for NaNbO<sub>3</sub>, NaTaO<sub>3</sub>, KNbO<sub>3</sub> and KTaO<sub>3</sub>, in good agreement with our experimental data. Table 4 collects the experimental energetics of LiTaO<sub>3</sub>, LiNbO<sub>3</sub>, NaTaO<sub>3</sub>, NaNbO<sub>3</sub>, KNbO<sub>3</sub> from the present study and those recently reported by us for KTaO<sub>3</sub><sup>54</sup>.

### (3) Stability of alkali tantalates and niobates

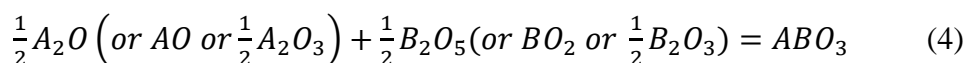
Figure 2 depicts the variation of formation enthalpies of LiTaO<sub>3</sub>, LiNbO<sub>3</sub>, NaTaO<sub>3</sub>, NaNbO<sub>3</sub>, KNbO<sub>3</sub> and KTaO<sub>3</sub> with respect to their tolerance factors. The tolerance factor,  $t$ , defines the structural stability, and is frequently referred in discussion related to the perovskites. The tolerance factors of individual perovskites can be obtained based on the following expression<sup>55</sup>:

$$t = \frac{r_A + r_O}{\sqrt{2}(r_B + r_O)} \quad (3)$$

Here,  $r_A$ ,  $r_B$ , and  $r_O$  refer to the ionic radii of A<sup>1+</sup>, B<sup>5+</sup> and O<sup>2-</sup>, respectively. The ionic radii were taken from Shannon's effective ionic radii table<sup>56</sup>, and the coordination of 6 is assumed for Li<sup>+</sup>,

8 for Na<sup>+</sup>, 12 for K<sup>+</sup> and 6 for Ta<sup>5+</sup> and Nb<sup>5+</sup>. In the ideal cubic perovskite structure, the ratio of the A – O bond length ( $r_A + r_O$ ) to the B – O length ( $r_B + r_O$ ) equals  $\sqrt{2}$ , and thus  $t = 1$ . When this condition deviates, the structure distorts largely via tilting of its BO<sub>6</sub> octahedra, and thereby departs from cubic symmetry<sup>57</sup>. With increase in tolerance factor of alkali tantalate and niobate perovskites formation enthalpies becomes more negative (Figure 2).

The energetics of perovskite oxides and their phase stability can be discussed based on acid-base concepts<sup>58, 59</sup>. The enthalpy of formation of a ternary oxide such as ABO<sub>3</sub> (where A-site is occupied by ions: A<sup>+</sup>, A<sup>2+</sup> and A<sup>3+</sup>, while B-site: B<sup>5+</sup>, B<sup>4+</sup>, B<sup>3+</sup>, respectively) from the binary constituent oxides (reaction in Equation 4) reflects the strength of the chemical bonds in the ternary oxide relative to those in the binary oxides.



In the case of a ternary ABO<sub>3</sub> oxides, the most stable compounds form when the most basic binary A oxides combine with the most acidic B oxides (oxygen ions transferred from the base to the acid oxides). The oxide acidity/basicity can be measured in terms of ionic potential of the metal cation,  $z/r$ , where  $z$  is the formal charge and  $r$  the ionic radius. The larger the  $z/r$  of the cation, the less basic or the more acidic its oxide<sup>57</sup>. Then, the stability of ABO<sub>3</sub> perovskites can be defined by a parameter so-called stability index (ratio of ionic potential),  $s$ , which is defined as a  $z/r$  ratio between B and A cations:

$$s = \frac{(z/r)_B}{(z/r)_A} \quad (5)$$

Figure 3 depicts the relation of the experimental enthalpies of formation,  $\Delta H_f^{\text{ox}}$ , of a number of perovskites as a function of  $s$ . Compounds from the present study are included (with KTaO<sub>3</sub> taken from Zlotnik *et al.*<sup>54</sup>), together with other perovskites from group III-III, II-IV and I-V (and additionally mixed II-IV and I-V). The III-III group is represented by the lanthanides<sup>60</sup>: LaAlO<sub>3</sub>, GdAlO<sub>3</sub>, YAlO<sub>3</sub>, DyAlO<sub>3</sub>, EuAlO<sub>3</sub>, LaGaO<sub>3</sub>, NdGaO<sub>3</sub>, LaFeO<sub>3</sub>, EuFeO<sub>3</sub>, GdFeO<sub>3</sub>, DyFeO<sub>3</sub> and LuFeO<sub>3</sub>, the II-IV group by the titanates and zirconates<sup>62</sup>: SrTiO<sub>3</sub>, CaTiO<sub>3</sub>, BaTiO<sub>3</sub>, PbTiO<sub>3</sub>, SrZrO<sub>3</sub>, CaZrO<sub>3</sub>, BaZrO<sub>3</sub> and PbZrO<sub>3</sub>, and the mixed II-IV and I-V group by (Na<sub>1-x</sub>Sr<sub>x</sub>)(Nb<sub>1-x</sub>Ti<sub>x</sub>)O<sub>3</sub><sup>30</sup>. Since an A oxide acts as a base and a B oxide as an acid, thus, the larger the  $s$  the more stable the perovskite, i.e. more exothermic is the enthalpy of formation of the ternary oxide from its binary constituents. It is clearly demonstrated in Figure 3 that with an increasing of  $s$ ,  $\Delta H_f^{\text{ox}}$  becomes more exothermic. The data for the III-III and mixed II-IV

and I-V perovskites fall well on the trend, but some compositions from the II-IV and I-V type somewhat deviate from the polynomial fitted line.

Figure 4 (a) shows variation of formation enthalpies of alkali tantalates and niobates with their surface energies, along with the reported formation enthalpies and surface energetics of selected perovskite titanates:  $\text{CaTiO}_3$ ,  $\text{SrTiO}_3$ ,  $\text{BaTiO}_3$  and  $\text{PbTiO}_3$ <sup>41,63</sup>. The perovskites having more exothermic enthalpies of formation,  $\Delta H_f^{\rho}$ , appear to have higher surface energies.  $\text{PbTiO}_3$  has a less exothermic integral enthalpy of water vapour adsorption, indicating a lower affinity of water and less hydrophilic character<sup>41, 63</sup>. It has been observed that the more ionic the perovskite, more exothermic the  $\Delta H_f^{\rho}$ , the higher its surface energy, and more tightly it binds  $\text{H}_2\text{O}$ <sup>55</sup>. The surface energy increases with increase of tolerance factor (Figure 4 (b)). The different surface energies of alkali tantalates and niobates are potentially important in the liquid phase synthesis of the nanoparticles, in particular influencing processes such as nucleation, growth, Ostwald ripening, and nanoparticle stabilization. The higher surface energy may accelerate nucleation and growth<sup>63</sup>.

#### 4. Conclusions

Alkali tantalates and niobates with perovskite-type structure,  $\text{LiTaO}_3$ ,  $\text{LiNbO}_3$ ,  $\text{NaTaO}_3$ ,  $\text{NaNbO}_3$  and  $\text{KNbO}_3$ , were synthesized by mixed oxide method and their formation enthalpies and surface energetics were determined by high-temperature oxide melt solution calorimetry. The formation enthalpy becomes more exothermic (higher thermodynamic stability) and surface energy increases with an increase in ionic radius of the A-site cation (Li, Na and K), or with the tolerance factor.

#### Acknowledgements:

Sulata K. Sahu and Alexandra Navrotsky acknowledge the U.S. Department of Energy, Office of Basic Energy Sciences, grant: DE-FG02-05ER15667 for financial support. Sebastian Zlotnik and Paula M. Vilarinho acknowledge FEDER funds via Programa Operacional Factores de Competitividade – COMPETE and National funds via FCT (Fundação para a Ciência e

Tecnologia) within the Project CICECO - FCOMP-01-0124-FEDER-037271 (FCT PEst-C/CTM/LA0011/2013) and individual FCT grant (SFRH/BD/67023/2009).

## References:

1. G. A. Geguzina, L. A. Reznitchenko and N. V. Dergunova, *Ferroelectrics*, 1998, **214**, 261-271.
2. C. N. W. Darlington and K. S. Knight, *Acta Crystallographica Section B*, 1999, **55**, 24-30.
3. S. Lanfredi, M. H. Lente and J. A. Eiras, *Applied Physics Letters*, 2002, **80**, 2731-2733.
4. V. Shanker, S. L. Samal, G. K. Pradhan, C. Narayana and A. K. Ganguli, *Solid State Sciences*, 2009, **11**, 562-569.
5. W. Wunderlich and B. Baufeld, in *Ceramic Materials*, ed. W. Wunderlich, InTech, 2010.
6. X. C. Tong, in *Advanced Materials for Integrated Optical Waveguides*, Springer International Publishing, 2014, pp. 335-376.
7. A. Huanosta and A. R. West, *Journal of Applied Physics*, 1987, **61**, 5386-5391.
8. T. Volk and M. Wohlecke, in *Lithium Niobate: Defects, Photorefraction and Ferroelectric Switching*, Springer-Verlag, Berlin Heidelberg, 2009, pp. 1-7.
9. K. Nakamura, T. Tokiwa and Y. Kawamura, *Journal of Applied Physics*, 2002, **91**, 9272-9276.
10. Y. Nakayama, P. J. Pauzauskie, A. Radenovic, R. M. Onorato, R. J. Saykally, J. Liphardt and P. Yang, *Nature*, 2007, **447**, 1098-1101.
11. R. Comes, M. Lambert and A. Guinier, *Solid State Communications*, 1968, **6**, 715-719.
12. G. A. Samara, *Journal of Physics: Condensed Matter*, 2003, **15**, R367.
13. R. G. Geyer, B. Riddle, J. Krupka and L. A. Boatner, *Journal of Applied Physics*, 2005, **97**, 104111.
14. J. Rödel, K. G. Webber, R. Dittmer, W. Jo, M. Kimura and D. Damjanovic, *Journal of the European Ceramic Society*, 2015, **35**, 1659-1681.
15. R. E. Jaeger and L. Egerton, *Journal of the American Ceramic Society*, 1962, **45**, 209-213.
16. J. F. Li, K. Wang, F. Y. Zhu, L. Q. Cheng and F. Z. Yao, *Journal of the American Ceramic Society*, 2013, **96**, 3677-3696.
17. F. Rubio-Marcos, J. J. Romero, M. S. Martín-Gonzalez and J. F. Fernández, *Journal of the European Ceramic Society*, 2010, **30**, 2763-2771.
18. Y. Li, J. Li, Z. Zhou, R. Guo and A. Bhalla, *Ferroelectrics*, 2011, **425**, 82-89.
19. E. Ringgaard and T. Wurlitzer, *Journal of the European Ceramic Society*, 2005, **25**, 2701-2706.
20. K.-i. Kakimoto, I. Masuda and H. Ohsato, *Journal of the European Ceramic Society*, 2005, **25**, 2719-2722.
21. D. Damjanovic, N. Klein, J. Li and V. Porokhonsky, *Functional Materials Letters*, 2010, **3**, 5-13.
22. S. SulataKumari and N. Alexandra, in *High Temperature Materials and Mechanisms*, CRC Press, 2014, pp. 17-38.
23. Z. H. Zeng, F. Calle-Vallejo, M. B. Mogensen and J. Rossmeisl, *Phys. Chem. Chem. Phys.*, 2013, **15**, 7526-7533.

24. K. S. Sahu, R. Ganesan and T. Gnanasekaran, *Journal of Nuclear Materials*, 2008, **376**, 366-370.
25. S. K. Sahu, R. Ganesan and T. Gnanasekaran, *The Journal of Chemical Thermodynamics*, 2010, **42**, 1-7.
26. S. K. Sahu, R. Ganesan and T. Gnanasekaran, *Journal of Nuclear Materials*, 2012, **426**, 214-222.
27. I. Pozdnyakova, A. Navrotsky, L. Shilkina and L. Reznitchenko, *Journal of the American Ceramic Society*, 2002, **85**, 379-384.
28. A. Popovič, L. Bencze, J. Koruza, B. Malič and M. Kosec, *International Journal of Mass Spectrometry*, 2012, **309**, 70-78.
29. D. Kobertz, M. Müller and A. Molak, *Calphad*, 2015, **48**, 55-71.
30. H. Xu, A. Navrotsky, Y. Su and M. L. Balmer, *Chemistry of Materials*, 2005, **17**, 1880-1886.
31. M. H. Frey and D. A. Payne, *Applied Physics Letters*, 1993, **63**, 2753-2755.
32. A. Navrotsky, *International Journal of Quantum Chemistry*, 2009, **109**, 2647-2657.
33. R. H. R. Castro and D. V. Quach, *The Journal of Physical Chemistry C*, 2012, **116**, 24726-24733.
34. A. Shigemi and T. Wada, *Japanese Journal of Applied Physics*, 2004, **43**, 6793.
35. A. Shigemi and T. Wada, *Japanese Journal of Applied Physics*, 2005, **44**, 8048.
36. A. Shigemi and T. Wada, *MRS Online Proceedings Library*, 2005, **902**.
37. J. M. McHale, A. Auroux, A. J. Perrotta and A. Navrotsky, *Science*, 1997, **277**, 788-791.
38. A. A. Levchenko, G. Li, J. Boerio-Goates, B. F. Woodfield and A. Navrotsky, *Chemistry of Materials*, 2006, **18**, 6324-6332.
39. P. Zhang, F. Xu, A. Navrotsky, J. S. Lee, S. Kim and J. Liu, *Chemistry of Materials*, 2007, **19**, 5687-5693.
40. A. V. Radha, O. Bomati-Miguel, S. V. Ushakov, A. Navrotsky and P. Tartaj, *Journal of the American Ceramic Society*, 2009, **92**, 133-140.
41. S. K. Sahu, P. S. Maram and A. Navrotsky, *Journal of the American Ceramic Society*, 2013, **96**, 3670-3676.
42. S. K. Sahu, R. Ganesan, T. G. Srinivasan and T. Gnanasekaran, *The Journal of Chemical Thermodynamics*, 2011, **43**, 750-753.
43. S. K. Sahu, R. Ganesan and T. Gnanasekaran, *The Journal of Chemical Thermodynamics*, 2013, **56**, 57-59.
44. S. K. Sahu, D. K. Unruh, T. Z. Forbes and A. Navrotsky, *Chemistry of Materials*, 2014, **26**, 5105-5112.
45. A. Navrotsky, C. Ma, K. Lilova and N. Birkner, *Science*, 2010, **330**, 199-201.
46. A. Navrotsky, *ChemPhysChem*, 2011, **12**, 2207-2215.
47. G. Pawley, *Journal of Applied Crystallography*, 1981, **14**, 357-361.
48. A. Navrotsky, *Physics and Chemistry of Minerals*, 1997, **24**, 222-241.
49. S. V. Ushakov and A. Navrotsky, *Applied Physics Letters*, 2005, **87**, 164103.
50. G. C. C. Costa, S. V. Ushakov, R. H. R. Castro, A. Navrotsky and R. Muccillo, *Chemistry of Materials*, 2010, **22**, 2937-2945.
51. S. Hayun, T. Y. Shvareva and A. Navrotsky, *Journal of the American Ceramic Society*, 2011, **94**, 3992-3999.
52. S. Körbel, P. Marton and C. Elsässer, *Physical Review B*, 2010, **81**, 174115.
53. L. A. Reznitskii, *Inorganic Materials*, 2001, **37**, 491-495.
54. S. Zlotnik, S. K. Sahu, A. Navrotsky and P. M. Vilarinho, *Chemistry – A European Journal*, 2015, **21**, 5231-5237.
55. V. M. Goldschmidt, *Naturwissenschaften*, 1926, **14**, 477-485.
56. R. Shannon, *Acta Crystallographica Section A*, 1976, **32**, 751-767.

57. A. Navrotsky, in *Physics and Chemistry of Earth Materials*, ed. A. Navrotsky, Cambridge University Press, 1994, pp. 172-272.
58. S. Stølen and T. Grande, in *Chemical Thermodynamics of Materials*, eds. S. Stølen, T. Grande and N. L. Allan, John Wiley & Sons, Ltd, 2004, pp. 197-227.
59. A. Navrotsky, *American Mineralogist*, 1994, **79**, 589.
60. Y. Kanke and A. Navrotsky, *Journal of Solid State Chemistry*, 1998, **141**, 424-436.
61. N. Kimizuka, A. Yamamoto, H. Ohashi, T. Sugihara and T. Sekine, *Journal of Solid State Chemistry*, 1983, **49**, 65-76.
62. E. Takayama-Muromachi and A. Navrotsky, *Journal of Solid State Chemistry*, 1988, **72**, 244-256.
63. G. C. C. Costa, P. Saradhi Maram and A. Navrotsky, *Journal of the American Ceramic Society*, 2012, **95**, 3254-3262.
64. R. A. Robie, B. S. Hemingway and J. R. Fisher, *Thermodynamic Properties of Minerals and Related Substances at 298.15K and 1 Bar (105 Pascals) Pressure and at Higher Temperatures*, U.S. Government Printing Office, 1978.

## Figure Captions

**Figure 1.** The XRD patterns of the alkali tantalates:  $\text{LiTaO}_3$  and  $\text{NaTaO}_3$ , and niobates:  $\text{LiNbO}_3$ ,  $\text{NaNbO}_3$  and  $\text{KNbO}_3$ , with perovskite-like structures synthesized via conventional solid-state reaction. In all cases the samples were detected to be monophasic, matching to the following JCPDS-PDF files: rhombohedral  $\text{LiTaO}_3$  to 01-087-2461 (SG:  $R3c$ ), rhombohedral  $\text{LiNbO}_3$  to 04-009-3436 (SG:  $R3c$ ), orthorhombic  $\text{NaTaO}_3$  to 04-010-2738 (SG:  $Pnma$ ), orthorhombic  $\text{NaNbO}_3$  to 04-014-2322 (SG:  $Pbcm$ ) and orthorhombic  $\text{KNbO}_3$  to 04-007-9572 (SG:  $Bmm2$ ). The major diffraction peaks are indexed.

**Figure 2.** Experimental data of formation enthalpies,  $\Delta H_f^{\text{ox}}$ , of alkali niobates and tantalates vs tolerance factor,  $t$ . Solid symbols correspond to data of the present study and open symbols to literature data. The formation enthalpy is more exothermic for the perovskites with tolerance factor close to the ideal cubic,  $t = 1$ .

**Figure 3.** Formation enthalpies,  $\Delta H_f^{\text{ox}}$ , of alkali tantalates and niobates (solid diamond symbols):  $\text{LiTaO}_3$ ,  $\text{LiNbO}_3$ ,  $\text{NaTaO}_3$ ,  $\text{NaNbO}_3$ ,  $\text{KNbO}_3$  and  $\text{KTaO}_3$ , together with other perovskites (open triangles for III-III, open circles for II-IV and open squares for mixed II-IV and I-V type perovskites, taken from literature) as a function of stability index (ratio of ionic potential),  $s$ . The curve represents a polynomial fit to all the data.

**Figure 4.** (a) Formation enthalpies of alkali niobate and tantalate together with  $\text{CaTiO}_3$ ,  $\text{SrTiO}_3$ ,  $\text{BaTiO}_3$  and  $\text{PbTiO}_3$  perovskites versus surface energies. The surface energy increases as the formation enthalpy becomes more exothermic. (b) Surface energies of alkali niobate and tantalate perovskites together with  $\text{CaTiO}_3$ ,  $\text{SrTiO}_3$ ,  $\text{BaTiO}_3$  and  $\text{PbTiO}_3$  versus tolerance factors. The  $\gamma_{\text{hyd}}$  increases with an increase of the  $t$ . Solid squares represent data from the present work and open circles literature data<sup>41, 63</sup>.

## Table Captions

**Table 1.** Characterization and thermochemical data for alkali tantalates:  $\text{LiTaO}_3$ ,  $\text{NaTaO}_3$ , and niobates:  $\text{LiNbO}_3$ ,  $\text{NaNbO}_3$  and  $\text{KNbO}_3$ .

**Table 2.** Thermochemical cycle used for water correction for as-synthesized nanocrystalline  $\text{LiTaO}_3$ ,  $\text{LiNbO}_3$ ,  $\text{NaTaO}_3$ ,  $\text{NaNbO}_3$  and  $\text{KNbO}_3$ .

**Table 3.** Thermochemical cycle used to calculate the formation enthalpies  $\text{LiTaO}_3$ ,  $\text{LiNbO}_3$ ,  $\text{NaTaO}_3$ ,  $\text{NaNbO}_3$  and  $\text{KNbO}_3$ .

**Table 4.** Tolerance factor and energetics of  $\text{LiTaO}_3$ ,  $\text{LiNbO}_3$ ,  $\text{NaTaO}_3$ ,  $\text{NaNbO}_3$ ,  $\text{KNbO}_3$  and  $\text{KTaO}_3$ .

Figure 1

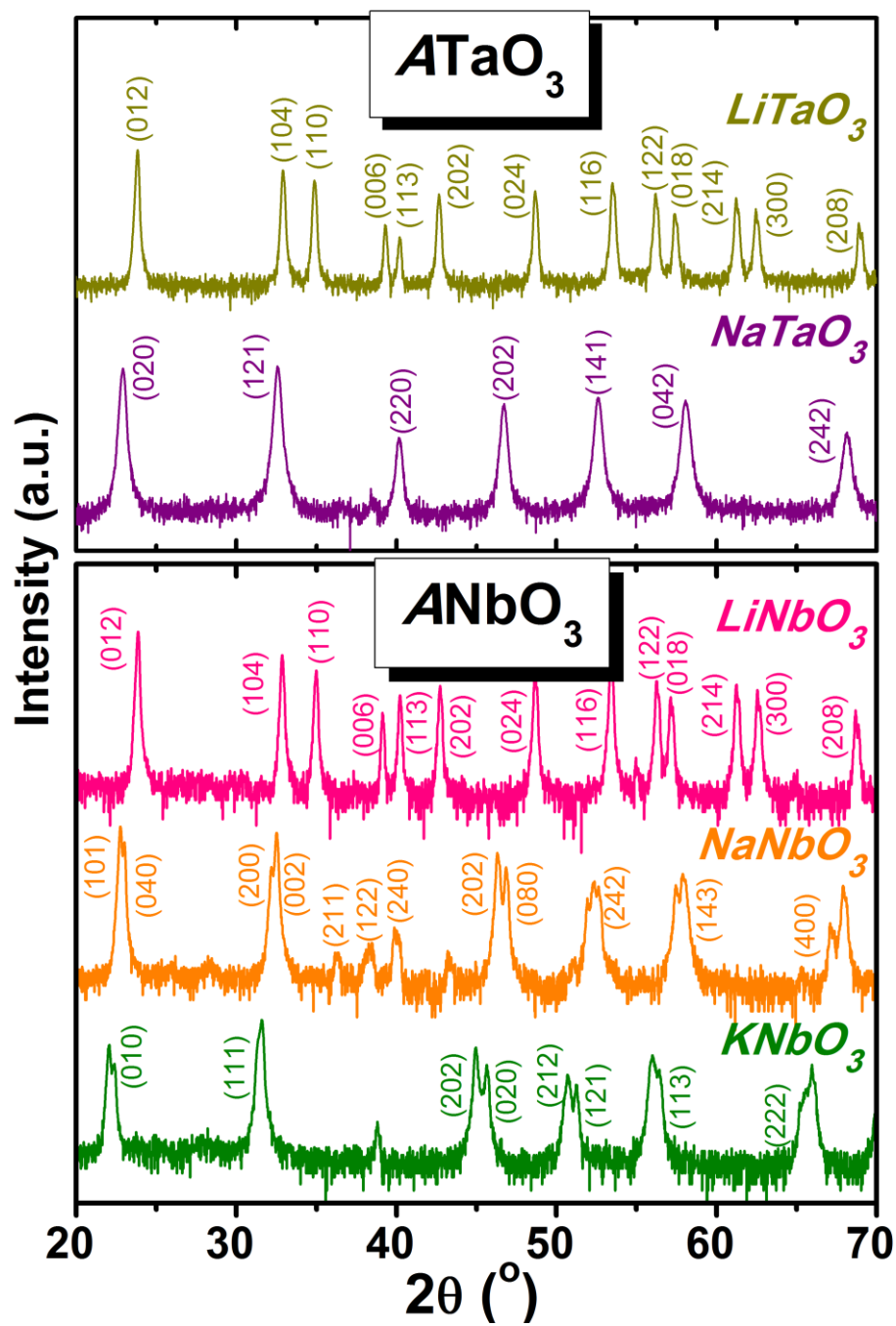


Figure 2

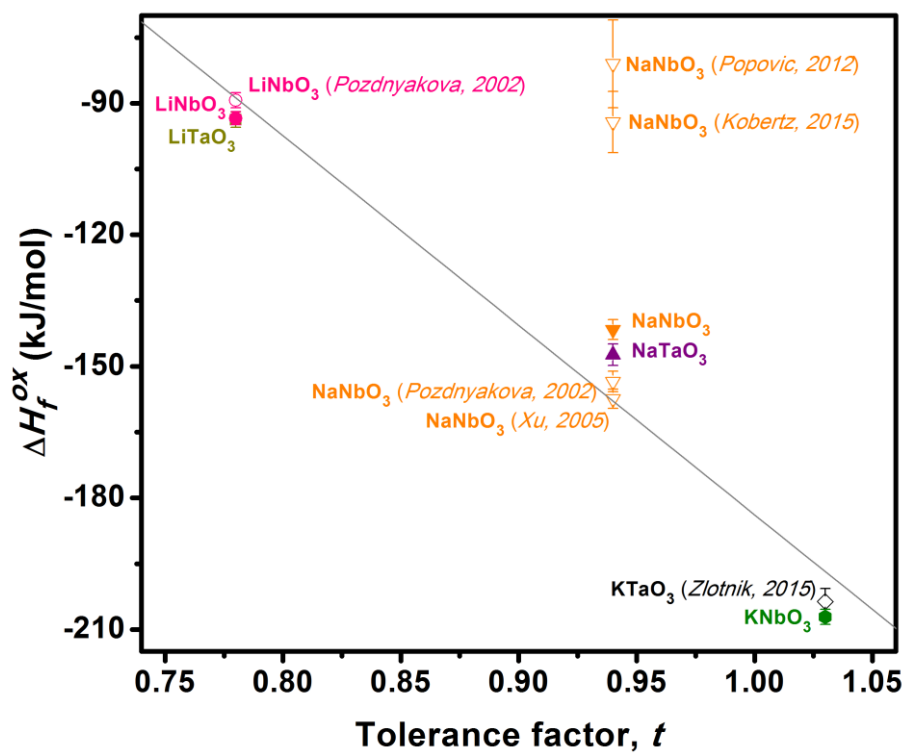


Figure 3.

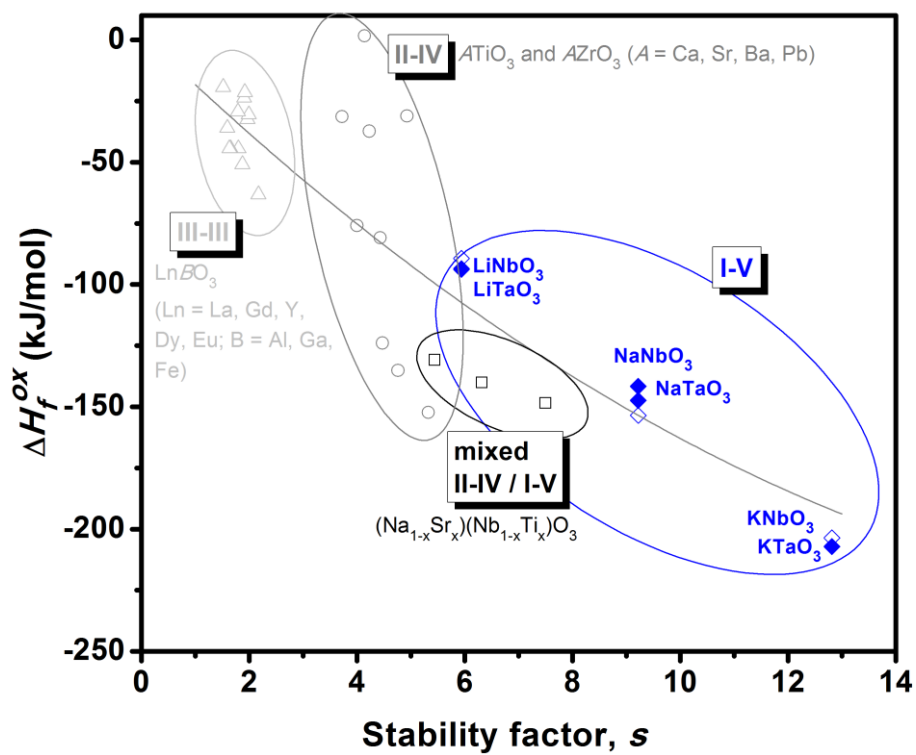


Figure 4 (a) and (b).

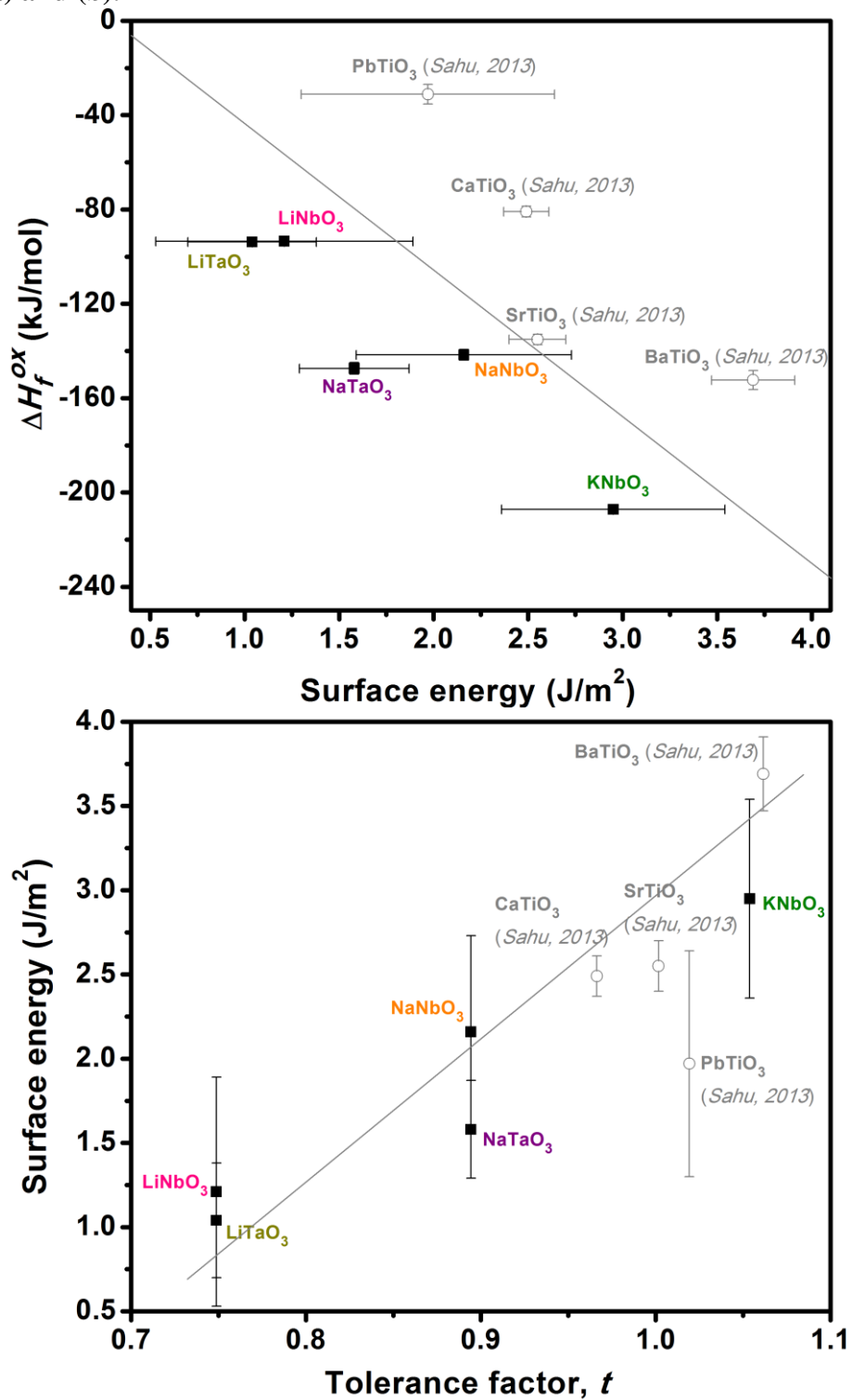


Table 1.

Table 1: Characterization and thermochemical data for alkali tantalates: LiTaO<sub>3</sub>, NaTaO<sub>3</sub>, and niobates: LiNbO<sub>3</sub>, NaNbO<sub>3</sub> and KNbO<sub>3</sub>.

	Surface area, $S_{BET}$ (m <sup>2</sup> /g)	Crystallite size, $\langle D \rangle$ (nm)		Water content, $n$ , in ABO <sub>3</sub> · $n$ H <sub>2</sub> O (moles)	$\Delta H_{ds}$ (kJ/mol)		Surface energy, $\gamma_{hyd}$ (J/m <sup>2</sup> ) (Hydrated surface)
		From XRD	From BET <sup>a</sup>		Bulk	Nano	
<b>LiTaO<sub>3</sub></b>	7.62 ± 0.38	100.7 ± 5.8	106.2	0.040	93.79 ± 0.43	91.91 ± 0.42	1.04 ± 0.34
<b>LiNbO<sub>3</sub></b>	4.17 ± 0.35	103.1 ± 2.5	103.9	0.021	95.27 ± 0.21	94.52 ± 0.36	1.21 ± 0.68
<b>NaTaO<sub>3</sub></b>	8.97 ± 0.54	47.4 ± 3.1	31.5	0.082	88.77 ± 0.44	85.19 ± 0.65	1.58 ± 0.29
<b>NaNbO<sub>3</sub></b>	6.42 ± 0.55	63.9 ± 2.1	68.2	0.025	84.83 ± 0.38	82.56 ± 0.42	2.16 ± 0.57
<b>KNbO<sub>3</sub></b>	5.97 ± 0.37	72.5 ± 3.6	70.1	0.037	95.10 ± 0.41	91.93 ± 0.44	2.95 ± 0.59

<sup>a</sup> Calculated from  $S_{BET}$ :  $\langle D \rangle = 6000 / (S_{BET} \cdot \rho)$ , using theoretical densities,  $\rho$ , of 7.415 g/cm<sup>3</sup> (LiTaO<sub>3</sub>, JCPDS-PDF 01-087-2461), 4.618 g/cm<sup>3</sup> (LiNbO<sub>3</sub>, JCPDS-PDF 04-009-3436), 7.089 g/cm<sup>3</sup> (NaTaO<sub>3</sub>, JCPDS-PDF 04-010-2738), 4.565 g/cm<sup>3</sup> (NaNbO<sub>3</sub>, JCPDS-PDF 04-014-2322), and 4.619 g/cm<sup>3</sup> (KNbO<sub>3</sub>, JCPDS-PDF 04-007-9572). Uncertainties are calculated as two standard deviations of the mean.

**Table 2.**

Table 2: Thermochemical cycle used for water correction for as-synthesized nanocrystalline LiTaO<sub>3</sub>, LiNbO<sub>3</sub>, NaTaO<sub>3</sub>, NaNbO<sub>3</sub> and KNbO<sub>3</sub>.

$ABO_3 \cdot nH_2O$ (solid, 25°C) $\rightarrow$ $ABO_3$ (soln., 702°C) + $nH_2O$ (gas, 702°C)	$\Delta H_1 = \Delta H_{ds}$
$nH_2O$ (gas, 702°C) $\rightarrow$ $nH_2O$ (gas, 25°C)	$\Delta H_2 = n (-25.1 \pm 0.1) \text{ kJ/mol}^{64}$
$nH_2O$ (gas, 25°C) $\rightarrow$ $nH_2O$ (liq., 25°C)	$\Delta H_3 = n (-44.0 \pm 0.1) \text{ kJ/mol}^{64}$
$ABO_3$ (solid, 25°C) $\rightarrow$ $ABO_3$ (soln., 702°C)	$\Delta H_4 = \Delta H_{ds} = \Delta H_1 + \Delta H_2 + \Delta H_3$

Soln. means dissolved in 3Na<sub>2</sub>O·4MoO<sub>3</sub>

Table 3.

Table 3: Thermochemical cycle used to calculate the formation enthalpies LiTaO<sub>3</sub>, LiNbO<sub>3</sub>, NaTaO<sub>3</sub>, NaNbO<sub>3</sub> and KNbO<sub>3</sub>.

	Reaction	Enthalpies (kJ/mol)
From oxides	(1) Li <sub>2</sub> O <sub>(xl, 25°C)</sub> → Li <sub>2</sub> O <sub>(soln, 702°C)</sub>	ΔH <sub>1</sub> = -90.3 ± 2.5
	(2) Na <sub>2</sub> O <sub>(xl, 25°C)</sub> → Na <sub>2</sub> O <sub>(soln, 702°C)</sub>	ΔH <sub>2</sub> = -207.56 ± 4.25
	(3) K <sub>2</sub> O <sub>(xl, 25°C)</sub> → K <sub>2</sub> O <sub>(soln, 702°C)</sub>	ΔH <sub>3</sub> = -318.0 ± 3.1
	(4) Ta <sub>2</sub> O <sub>5 (xl, 25°C)</sub> → Ta <sub>2</sub> O <sub>5 (soln, 702°C)</sub>	ΔH <sub>4</sub> = 90.41 ± 2.5
	(5) Nb <sub>2</sub> O <sub>5 (xl, 25°C)</sub> → Nb <sub>2</sub> O <sub>5 (soln, 702°C)</sub>	ΔH <sub>5</sub> = 93.97 ± 1.6
	(6) LiTaO <sub>3 (xl, 25°C)</sub> → ½ Li <sub>2</sub> O <sub>(soln, 702°C)</sub> + ½ Ta <sub>2</sub> O <sub>5 (soln, 702°C)</sub>	ΔH <sub>6</sub> = 93.79 ± 0.43
	(7) LiNbO <sub>3 (xl, 25°C)</sub> → ½ Li <sub>2</sub> O <sub>(soln, 702°C)</sub> + ½ Nb <sub>2</sub> O <sub>5 (soln, 702°C)</sub>	ΔH <sub>7</sub> = 95.27 ± 0.31
	(8) NaTaO <sub>3 (xl, 25°C)</sub> → ½ Na <sub>2</sub> O <sub>(soln, 702°C)</sub> + ½ Ta <sub>2</sub> O <sub>5 (soln, 702°C)</sub>	ΔH <sub>8</sub> = 88.77 ± 0.44
	(9) NaNbO <sub>3 (xl, 25°C)</sub> → ½ Na <sub>2</sub> O <sub>(soln, 702°C)</sub> + ½ Nb <sub>2</sub> O <sub>5 (soln, 702°C)</sub>	ΔH <sub>9</sub> = 84.83 ± 0.38
	(10) KNbO <sub>3 (xl, 25°C)</sub> → ½ K <sub>2</sub> O <sub>(soln, 702°C)</sub> + ½ Nb <sub>2</sub> O <sub>5 (soln, 702°C)</sub>	ΔH <sub>10</sub> = 95.10 ± 0.41
	(11) ½ Li <sub>2</sub> O <sub>(soln, 702°C)</sub> + ½ Ta <sub>2</sub> O <sub>5 (soln, 702°C)</sub> → LiTaO <sub>3 (xl, 25°C)</sub>	ΔH <sub>11</sub> = -93.74 ± 1.77
	(12) ½ Li <sub>2</sub> O <sub>(soln, 702°C)</sub> + ½ Nb <sub>2</sub> O <sub>5 (soln, 702°C)</sub> → LiNbO <sub>3 (xl, 25°C)</sub>	ΔH <sub>12</sub> = -93.44 ± 1.48
	(13) ½ Na <sub>2</sub> O <sub>(soln, 702°C)</sub> + ½ Ta <sub>2</sub> O <sub>5 (soln, 702°C)</sub> → NaTaO <sub>3 (xl, 25°C)</sub>	ΔH <sub>13</sub> = -147.35 ± 2.46
	(14) ½ Na <sub>2</sub> O <sub>(soln, 702°C)</sub> + ½ Nb <sub>2</sub> O <sub>5 (soln, 702°C)</sub> → NaNbO <sub>3 (xl, 25°C)</sub>	ΔH <sub>14</sub> = -141.63 ± 2.27
	(15) ½ K <sub>2</sub> O <sub>(soln, 702°C)</sub> + ½ Nb <sub>2</sub> O <sub>5 (soln, 702°C)</sub> → KNbO <sub>3 (xl, 25°C)</sub>	ΔH <sub>15</sub> = -207.12 ± 1.74

From elements	(16) $2\text{Li}_{(\text{xl}, 25^\circ\text{C})} + \frac{1}{2} \text{O}_2 \rightarrow \text{Li}_2\text{O}_{(\text{xl}, 25^\circ\text{C})}$	$\Delta H_{16} = -597.9$
	(17) $2\text{Na}_{(\text{xl}, 25^\circ\text{C})} + \frac{1}{2} \text{O}_2 \rightarrow \text{Na}_2\text{O}_{(\text{xl}, 25^\circ\text{C})}$	$\Delta H_{17} = -414.8$
	(18) $2\text{K}_{(\text{xl}, 25^\circ\text{C})} + \frac{1}{2} \text{O}_2 \rightarrow \text{K}_2\text{O}_{(\text{xl}, 25^\circ\text{C})}$	$\Delta H_{18} = -358.02 \pm 3.74$
	(19) $2\text{Ta}_{(\text{xl}, 25^\circ\text{C})} + \frac{1}{2} \text{O}_2 \rightarrow \text{Ta}_2\text{O}_5(\text{xl}, 25^\circ\text{C})$	$\Delta H_{19} = -2046.5 \pm 4.2$
	(20) $2\text{Nb}_{(\text{xl}, 25^\circ\text{C})} + \frac{1}{2} \text{O}_2 \rightarrow \text{Nb}_2\text{O}_5(\text{xl}, 25^\circ\text{C})$	$\Delta H_{20} = -1899.54 \pm 1.5$
	<b>(21) <math>\text{Li}_{(\text{xl}, 25^\circ\text{C})} + \text{Ta}_{(\text{xl}, 25^\circ\text{C})} + 3/2 \text{O}_2 \rightarrow \text{LiTaO}_3(\text{xl}, 25^\circ\text{C})</math></b>	<b><math>\Delta H_{21} = -1415.94 \pm 2.29</math></b>
	<b>(22) <math>\text{Li}_{(\text{xl}, 25^\circ\text{C})} + \text{Nb}_{(\text{xl}, 25^\circ\text{C})} + 3/2 \text{O}_2 \rightarrow \text{LiNbO}_3(\text{xl}, 25^\circ\text{C})</math></b>	<b><math>\Delta H_{22} = -1342.16 \pm 1.72</math></b>
	<b>(23) <math>\text{Na}_{(\text{xl}, 25^\circ\text{C})} + \text{Ta}_{(\text{xl}, 25^\circ\text{C})} + 3/2 \text{O}_2 \rightarrow \text{NaTaO}_3(\text{xl}, 25^\circ\text{C})</math></b>	<b><math>\Delta H_{23} = -1378.00 \pm 3.27</math></b>
	<b>(24) <math>\text{Na}_{(\text{xl}, 25^\circ\text{C})} + \text{Nb}_{(\text{xl}, 25^\circ\text{C})} + 3/2 \text{O}_2 \rightarrow \text{NaNbO}_3(\text{xl}, 25^\circ\text{C})</math></b>	<b><math>\Delta H_{24} = -1298.80 \pm 2.52</math></b>
	<b>(25) <math>\text{K}_{(\text{xl}, 25^\circ\text{C})} + \text{Nb}_{(\text{xl}, 25^\circ\text{C})} + 3/2 \text{O}_2 \rightarrow \text{KNbO}_3(\text{xl}, 25^\circ\text{C})</math></b>	<b><math>\Delta H_{25} = -1335.90 \pm 2.73</math></b>

where:  $\Delta H_{11} = \frac{1}{2} \Delta H_1 + \frac{1}{2} \Delta H_4 - \Delta H_6$ ,  $\Delta H_{12} = \frac{1}{2} \Delta H_1 + \frac{1}{2} \Delta H_5 - \Delta H_7$ ,  $\Delta H_{13} = \frac{1}{2} \Delta H_2 + \frac{1}{2} \Delta H_4 - \Delta H_8$ ,  $\Delta H_{14} = \frac{1}{2} \Delta H_2 + \frac{1}{2} \Delta H_5 - \Delta H_9$ ,  $\Delta H_{15} = \frac{1}{2} \Delta H_3 + \frac{1}{2} \Delta H_5 - \Delta H_{10}$ ,  $\Delta H_{21} = \frac{1}{2} \Delta H_{16} + \frac{1}{2} \Delta H_{19} + \Delta H_{11}$ ,  $\Delta H_{22} = \frac{1}{2} \Delta H_{16} + \frac{1}{2} \Delta H_{20} + \Delta H_{12}$ ,  $\Delta H_{23} = \frac{1}{2} \Delta H_{17} + \frac{1}{2} \Delta H_{19} + \Delta H_{13}$ ,  $\Delta H_{24} = \frac{1}{2} \Delta H_{17} + \frac{1}{2} \Delta H_{20} + \Delta H_{14}$ , and  $\Delta H_{25} = \frac{1}{2} \Delta H_{18} + \frac{1}{2} \Delta H_{20} + \Delta H_{15}$ .

Table 4.

Table 4: Tolerance factor and energetics of LiTaO<sub>3</sub>, LiNbO<sub>3</sub>, NaTaO<sub>3</sub>, NaNbO<sub>3</sub>, KNbO<sub>3</sub> and KTaO<sub>3</sub>.

	LiTaO <sub>3</sub>	LiNbO <sub>3</sub>	NaTaO <sub>3</sub>	NaNbO <sub>3</sub>	KNbO <sub>3</sub>	KTaO <sub>3</sub> <sup>54</sup>
Tolerance factor, $t$	0.78	0.78	0.94	0.94	1.03	1.03
Formation enthalpy from oxides, $\Delta H_f^{ox}$ (kJ/mol)	$-93.74 \pm 1.77$	$-93.44 \pm 1.48$	$-147.35 \pm 2.46$	$-141.63 \pm 2.27$	$-207.12 \pm 1.74$	$-203.63 \pm 2.92$
Formation enthalpy from elements, $\Delta H_f^0$ (kJ/mol)	$-1415.94 \pm 2.29$	$-1342.16 \pm 1.72$	$-1378.00 \pm 3.27$	$-1298.80 \pm 2.52$	$-1335.90 \pm 2.73$	$-1408.23 \pm 3.75$
Hydrated surface energy, $\gamma_{hyd}$ (J/m <sup>2</sup> )	$1.04 \pm 0.34$	$1.21 \pm 0.68$	$1.58 \pm 0.29$	$2.16 \pm 0.57$	$2.95 \pm 0.59$	-